Similar and dissimilar lap friction stir welding of titanium alloys: on the elimination of the hook defect

Similar and dissimilar lap friction stir welding of titanium alloys: on the elimination of the hook defect

Similar and Dissimilar Lap Friction Stir Welding of Titanium Alloys: on the elimination of the hook defect

Vincenzo Lunetto*, Manuela De Maddis, Pasquale Russo Spena

Department of Management and Production Engineering, Politecnico di Torino, Corso Duca degli Abruzzi 24, 10129 Torino, Italy

* Corresponding author

Email: vincenzo.lunetto@polito.it

Abstract

This work investigates similar and dissimilar lap FSW of commercially pure titanium (CP-Ti) and Ti6Al4V sheets welded with two different tool shapes, truncated conical and enlarged pin heads. It aims to assess the influence of the two tools on the formation of the hook defects, mechanical strength, and fracture mode. The spindle torque and vertical force have also been monitored during the experimental FSW tests to relate the welding practice to each joint configuration. The joint strength of the FSW joints has been compared with that of joints obtained with laser welding to compare them with the most competitive fusion welding technique. The welding data have shown that the spindle torque and vertical force are related to the upper sheet strength and thermal conductivity. The dissimilar joints were particularly affected from the hook defects when welded with the truncated conical pin tool. This phenomenon was highlighted in the AS for the Ti6Al4V/CP-Ti joints and in the RS for the CP-Ti/ Ti6Al4V joints due to asymmetrical material flow between AS and RS and to the different material properties of the two alloys. The hook defect is absent in the joints obtained with the enlarged pin tool due to the more vigorous metal stirring. However, these welds gave a higher variability during the tensile test which was traced back to the superior variability in the monitored vertical force (from 10 kN to 23 kN). This evidence suggests the difficulty of adopting complex tool features in FSW of high strength-to-mass ratio materials as noticed from the "built up edge'' in the enlarged pin tool at the end of the weld.

Keywords: Friction Stir Welding; Tool Geometry; Laser Welding; Commercially Pure titanium; Ti6Al4V; Welding Data Monitoring; Joint Strength.

1. Introduction

Titanium alloys guarantee an excellent combination of such properties as a high strength-to-mass ratio, high fatigue resistance, and outstanding corrosion resistance [1–3]. Because of these features, titanium alloys play a specific role in many applications, ranging from the aerospace to the medical and chemical industries [4].

Different fusion welding techniques, including gas tungsten arc, plasma arc, electron beam, and laser welding, are generally used to weld titanium alloys. However, these type of titanium welds normally suffer from residual stresses, porosity, and coarse and brittle microstructures. On the other hand, friction stir welding (FSW), being a solid-state welding process, can overcome or limit these disadvantages because of the low heat input involved in the joining process [5–7]. For instance, Mehdi et al. [8] measured longitudinal

residual stresses going from -400 MPa close to the base material (BM) and up to 300 MPa in the heat affected zone (HAZ) of Ti6Al4V joints obtained by means of TIG welding. On the other hand, Edwards et. al. [9] measured longitudinal residual stress above -200 MPa close to the BM, below 200 MPa in the transition region and above -100 MPa in the centerline for FSW joint of the same titanium alloys. Moreover, unlike fusion welding technologies, FSW does not require additional materials (i.e., fillers) and avoids metal splatters, fumes, and solidification cracks [10]. Life Cycle Assessment (LCA) studies [11] have demonstrated that FSW reduces greenhouse gas emissions by about 30 % compared to traditional arc welding.

FSW is a solid-state welding process patented in 1991 by The Welding Institute (Cambridge, UK). The technology takes advantage of the heat input and the strain rate generated by the friction between a rotating tool and the materials that must be joined. As described by Mishra and Ma [12], this effect fulfills the different tasks required to create a weldment: (i) heating and softening of the materials, (ii) their stirring to create an intimate mixture, and (iii) forging of the weld surface. To broaden the adoption of FSW in manufacturing fields, three inherent issues - back support, weld thinning, and keyhole defects - should be addressed to ensure the structural integrity, safety, and service life of the FSW-assembled products. Meng et. al. [13] have reviewed the control strategies to prevent these issues and, hence, to improve the quality of FSW joints in terms of geometric dimensioning and tolerancing, and mechanical properties.

FSW is currently a well-established technique to join such light materials as aluminum alloys. However, the weldability of high-strength metals is still challenging. In general, these issues are mainly due to: (i) the high wear rate of the friction tools, (ii) the high cost and scarce availability of the necessary tools, (iii) the narrow process window, and (iv) the use of custom fixturing systems, especially for complex joint geometries [14]. Furthermore, focusing on titanium alloys, researchers are currently developing customized microstructures which can provide a transformation induced plasticity just like happens for TRIP steels exploiting the retained β phase [15]. As consequence, weldability of these materials should be tested in parallel to these new achievements in metallurgy. The FSW of commercially pure titanium (CP-Ti) and Ti6Al4V is of great interest since they are the most used titanium alloys in industry. For instance, CP-Ti is widely used in chemical engineering and construction of civil buildings for its resistance to corrosion and oxidation [16]. Moreover, despite the wide availability of several titanium alloys, the Ti6Al4V grade accounts for at least 50 % of the whole titanium market [17] thank to its capability to provide high weights savings in aerospace and urban mobility if adequate redesign procedures are implemented [18,19].

Reshad et al. [20] investigated the effects of the tilt angle, tool geometry, and material on the butt joining of 3 mm thick CP-Ti sheets. The results discouraged the use of high-speed steel (HSS) tools because of the severe wear and fracturing of the pin and shoulder nose. More resistant truncated conical WC pins were used to overcome these issues, but threaded WC pins continued to suffer from rapid wear and induced residual stress that was too high in the welded joint. The FSW joints exhibited a significant scattering of the tensile data, with a lower tensile strength, from 75 to 400 MPa, and a more limited elongation at fracture, from 2 to about 25 %, than the base metal, BM, (400 MPa and 39 %). Liu et al. [21–23] tried to determine a process

window to obtain defect-free FSW joints in 2 mm thick CP-Ti sheets by varying the tool rotational speed and the welding speed. They got defect-free welds using a 50-80 mm/min welding speed and a rotational speed in the 200-300 rpm range. The maximum shear tension strength of the joints was 14.5 kN (sample width 20 mm, with a sheet overlap of 45 mm), and the final fracture occurred in the BM. Liu et al. [22] also found a grain refinement from 22 to 6 μm and an increase in hardness from 150 to 175 HV when moving from the BM to the stir zone (SZ). Zhang et al. [24] used a PCBN tapered shoulder to butt weld 3 mm thick CP-Ti sheets. The tool left PCBN debris and Ti borides inside the joint, which led to a hardness peak in the SZ. Moreover, the authors did not find a clear thermo-mechanical affected zone (TMAZ) and highlighted a change in the microstructure grain size throughout the joint: 27 μm in the BM, 30 μm in the HAZ, and 13 μm in the SZ. Du et al. [25] used butt FSW to weld a 5 mm thick Ti4Al0.005B (TA5, α phase) alloy. The FSW joints were affected by a cavity defect located on the sheets bottom side. A backing plate made of titanium solved this issue. The low thermal conductivity of the Ti backing plate contained the heat input to the joining area, thus improving the material flow and stirring. TA5 showed a significant increase in hardness due to strain hardening, which increased from 275 to 425 HV, when moving from the BM to the SZ. Furthermore, notable grain refining was observed in the SZ, with an average grain size of about 1 μm. Amirov et al. [26] investigated the FSW butt joining of 2.5 mm thick Ti1.5Al1Mn (near α alloy) sheets. According to the previous experience, the authors conducted different experiments with α titanium alloys, with the following settings: 9.5-26 kN of vertical force, 400-950 rpm of rotational speed, and 90-180 mm/min of welding speed. The tests revealed that the vertical force had to be increased to above 25 kN, while the rotational speed had to be decreased to below 400 rpm due to the presence of percentages of β phase below the 2 % in the near α alloy respect to an α alloy.

The FSW of Ti6Al4V (α+β titanium alloy) has also been investigated in the literature. Ji and Li [27] performed the lap FSW of 1.8 mm thick Ti6Al4V to reduce the hook defect. Hooking is the most common defect in FSW lap joints, and it consists of an upward bending of the sheet interface caused by the tool plunging into the bottom sheet, which results in an upward movement of the metal from the bottom sheet to the top one. This leaves a hook in the upper sheet that, acting as a stress concentration factor, reduces the strength and ductility of the FSW joints. The authors found a primary and a secondary hook on the advancing side (AS) of the joint, with the latter being the nucleation site of the crack and then its propagation path. A maximum shear tension strength of 17 kN (sample width 20 mm, with a sheet overlap of 40 mm) and a slight increase in hardness were measured when moving from the BM (330 HV) to the SZ (375 HV). Buffa et al. [28] evaluated the effect of an increasing specific thermal contribution on the phase distribution and microstructure of the lap joints between 1.25 mm thick sheets. By using a progressive increase in the rotational speed and reducing the welding speed, the SZ was mainly characterized by an α+β structure. A predominant α and very fine α structure formed in the SZ when the thermal input was reduced. Maximum tensile strength of 750 MPa was found when the joints were welded with 700 rpm at 25 mm/min. Strengths of 500 MPa and 350 MPa were obtained for 500 rpm and 50 mm/min and for 300 rpm and 75 mm/min, respectively. Zhang et al. [29] conducted a butt FSW of 3 mm thick Ti6Al4V sheets. They found an increase

in the grain size for the α phase from 5 to 13 μm (about 35 μm for the BM) when increasing the rotational speed from 300 to 600 rpm. The tensile strength of the joints decreased slightly to 900 MPa (BM 950 MPa), while the elongation reduced from 10 % to about 6 % (BM 20 %). Edwards et al. [30] investigated the weldability of Ti6Al4V butt welds from 3, 6, 9, and 12 mm thick sheets and offered some recommendations on the tool design for each joint configuration. The experimental study showed a welding window with a rotational speed ranging from 150 to 325 rpm and a welding speed ranging from 60 to 110 mm/min. The largest thermal gradient and heat input were found for the thickest joints, and they were associated with an increase in the grain size of the joints as the joint thickness increased. An average tensile strength of 1025 MPa was obtained. Edwards et al. [31] butt welded Ti6Al4V 6 mm thick sheets and employed a tracer material (75 wt.% W, 25 wt.% Re blend powder 20 μm in size) to evaluate the material flow during FSW. The authors found that low rotational speed-to-traversing speed ratios (cold welds) resulted in a wide spread of the tracer material over the width but not over the thickness. The opposite behavior was observed when they used high rotational speed-to-traversing speed ratios (hot welds). Finally, Buffa et al. [32,33] employed a FEM simulation to study the lap and butt FSW of Ti6Al4V. The temperature and the effective strain distribution in the joint were predicted as a function of the welding and rotational speeds [32]. These data were then employed to predict the distribution of the α, α+β and β phases at various distances from the weld center to the BM [33]. They found a broader gradient for the β phase of a hot weld (peak value above 80 %) than for a cold joint (peak value below 30 %).

Most of the literature has focused on the FSW of similar titanium alloys. However, there is increasing interest in welding different titanium grades (in the petroleum, energy power, and aerospace fields, etc.) to obtain complementary advantages from the two joined metals. Gangwar et al. [34] investigated the butt FSW of two 4 mm thick α+β alloys (TIMET-54M and ATI-425). The study highlighted that the SZ is mainly characterized by refined prior β grains and finer acicular α when the alloy with a lower β-transus temperature (e.g., TIMET-54M) is placed on the AS. On the other hand, the SZ was characterized by coarser α lamellae for grain boundary α, when the same material was placed on the RS. Gonser [35] investigated the microstructure and mechanical properties of the butt FSW of Ti6Al4V and Timetal 21S (Ti-15 Mo-3 Nb-3 Al-0.2 Si) alloys. The results showed that the tensile strength and elongation at fracture of the FSW joints depended on the welding parameters and the placement of the alloy. The best mechanical properties were obtained for slower rotation and faster welding speeds (i.e., a lower heat input). The tensile fracture locations were observed in the lower resistant Timetal 21S alloy, its TMAZ, or the SR zone. Buhl et al. [36] evaluated the microstructural and mechanical properties of similar and dissimilar CP-Ti and Ti6Al4V alloy joints. They found that the mechanical strength of the joints was directly related to the lower resistant alloy, CP-Ti. CP-Ti welds showed a yield point and tensile strength of 345 and 450 MPa.

From the state-of-the-art literature two fields of investigations can be drawn. 1) The influence of the mixing of Ti alloys with different mechanical properties and the effect of the position of the Ti alloy (as the bottom or upper sheet) in a lap joint configuration on the mechanical strength and fracture mode still needs to be

fully understood. 2) The presence of the hook defect in lap FSW welds still represents a challenge to win especially in dissimilar joints.

Therefore, this work has aimed to investigate these two topics. More in details, a truncated conical and enlarged pin tools have been used in the experimental tests to differently treat the weld interface. The spindle torque and the vertical force were also monitored during the FSW experimental tests to establish possible relationships between the joining practice and the FSW joint performances.

2. Materials and methods

Titanium CP-Ti (grade 2) and Ti6Al4V (grade 5) annealed sheets with a nominal thickness of 2 mm have been examined in this study. The two alloys satisfied the standard ASTM B265 [37], as shown in Table 1. The CP-Ti had a typical full α phase and an average grain size of about 10-15 μm. The microstructure of Ti6Al4V was made up of α and β phases, with volume fractions of about 70 % and 30 %, respectively. A lack of martensitic structures was detected in the Ti6Al4V BM. The average grain size was about 10 μm for the α phase and 5 μm for the β phase. The CP-Ti and Ti6Al4V BMs showed hardness values of 160 and 330 HV0.5, respectively.

	Ti	Al	V	Fe	O	C	N	H
CP-Ti	Bal.	-	-	0.07	0.13	0.00	0.00	0.000
Ti6Al4V	Bal.	6.00	3.90	0.11	0.14	0.02	0.01	0.002

Table 1. Chemical composition (wt.%) for the two titanium alloys [37].

During FSW, the tool shape and the temperature field influence the metal flow. Based on the literature, a truncated conical tool geometry was designed to have a suitable combination of mechanical performances and a low wear rate at the tool edges. Table 2 summarizes the dimensions and features of the FSW tools used in the FSW of titanium alloys found in the reviewed literature. A truncated cone geometry was employed for the pin profile because such geometry helps to control the heat flow along the joint thickness direction and promotes a high hydrostatic pressure in the weld zone, Figure 1 a). FSW tools with threaded cones and threaded cylinders are often used to improve the stirring and flow of material, but they were not used in this study due to the excessive wear rate observed during some preliminary pilot tests. A flat shoulder was also selected to prevent excessive tool wear of sharp corners, which is generally observed for convex and tapered shoulders. A tungsten-rhenium alloy (75 wt.% W, 25 wt.% Re) was employed for the tools to withstand the elevated temperatures that are reached during the welding process. A pin length of 2 mm and a fixed plunge depth of 2.4 mm (position control mode) were chosen for the tools to penetrate the pin in the lower sheet and the shoulder in the upper sheet of 0.4 mm. A preliminary pilot experimental campaign revealed that a plunge depth of 2.3 mm can generate an interfacial failure of the welds. Moreover, a reduced length of the pin would require an excessive penetration of the shoulder inside the joint and a consequent rise in the produced flash. The preliminary pilot experimental campaign also identified the plunge speed and the dwell time, which were selected with the target to avoid an excessive vertical load against the FSW machine head. A relative

low ratio between the rotational speed [rpm] and the welding speed [mm/min] of 3.33 was used to avoid excessive heating of the joint. Table 3 shows the settings of the welding parameters and the four different lap joint configurations used in the experimental campaign.

The tool design also has a key role in alleviating hook defects. According to Huang et al. [38,39], this defect could be prevented in Al/Al and Al/steel lap joints with the use of an enlarged pin head with circumferential notches. The centripetal flow induced by the concave shape of the pin was beneficial to accelerating the flow behavior of the softening metals, which further increased the effective interfacial width between the two sheets and avoided interfacial defects of the lap joint. Based on these results, a tool with an enlarged pin head has also been used, Figure 1 b). The enlarged pin head shows a ring with a thickness large enough to extent its action for 0.38 mm and 0.25 mm respectively above and below the weld interface.

Sheet materials	Thicknesses	Tool material	Tool geometry		Reference
			Shoulder	Pin	
Commercially pure Ti, B	3	Pin: HSS or WC; Shoulder: HSS	18, F	PL:2.85, BD:5, TCy	[20]
Commercially pure Ti, B	3	Pin: WC; Shoulder: W	18, F	PL:2.85, BD:5, Cy	[20]
Commercially pure Ti, B	3	PCBN	15, T(166*)	PL:1.7, BD:5.1, T(90*)	[24]
Commercially pure Ti, L	2	WC-Co-based	15, F	PL:2, BD:6, Cy	[21]
Commercially pure Ti, L	2	WC-Co-based	15, F	PL:2, BD:6, Cy, SCS	[22]
Commercially pure Ti, L	2	WC-Co-based	15, F	PL:1.8-2.2, BD:6, Cy, SCS	[23]
Ti4Al0.005B (TA5), B	5	Co-based	18, T(174*)	PL:4.85, BD:8, T(45*)	[25]
Ti4Al0.005B (TA5), B	6	W-based	18, **	PL:5.8, BD:N.A., **	[40]
Ti4Al0.005B (TA5), B	4	Co-based	18, T	PL:3.8, BD:N.A., T	[41]
Ti4Al0.005B (TA5), Tj	4.2	N.A.	16, F	PL:4, BD:9, T(64*)	[10]
Ti1.5Al1Mn, B	2.5	ZhS6U	20, **	PL:2.4, BD:~5.7, T(60*)	[26]
Ti6Al4V, B	2	Pin: WRe(25%wt); Shoulder: GH4043	28, F	PL:1.9, BD:16, T(55*)	[42]
Ti6Al4V, B	2	Pin: WRe(25%wt); Shoulder: GH4043	26, F	PL:1.9, BD:16, T(55*)	[43]
Ti6Al4V, B	2	WRe(25%wt)	15, F	PL:N.A., BD:5, Cy	[44]
Ti6Al4V, B	2	WC-based	15, F	PL:1.8, BD:6, **	[45]
Ti6Al4V, B	3	W-La_2O_3(1%wt)	14, F	Pinless tool	[46]
Ti6Al4V, B	3	WLa-based	19, F	PL:2.8, BD:N.A., T	[30]
Ti6Al4V, B	6	WLa-based	24, F	PL:5.9, BD:N.A., T	[30]
Ti6Al4V, B	9	WLa-based	24, F	PL:9, BD:N.A., T	[30]
Ti6Al4V, B	12	WLa-based	32, F	PL:13.3, BD:N.A., T	[30]
Ti6Al4V, L	1.8	WRe-based	12, T	PL:1.9, BD:6.3, T(~55*), TC	[27]
Ti6Al4V, L	1.25	WRe(25%wt)	13, F	PL:2, BD:4, T(60*)	[28]
Ti6Al4V, B, Nu	3	WRe(25%wt)	16, **	PL:2.6, BD:5, T(60*)	[33]
Ti6Al4V, B, Nu	3	WC-based	16, **	PL:2.6, BD:5, T(60*)	[47]
Ti6Al4V, B, Nu	3	K10, K10-K30, WRe(25%wt)	16, F	PL:2.6, BD:5, T(60*)	[48]
Ti6Al4V, B, Nu	2	N.A.	12, F	PL:1.8, BD:6, T(~58*)	[49]

Ti6Al4V, B, Nu	2	WRe-based	12, **	PL:1.7, BD:8, T(~99*)	[50]
Ti6Al4V, L, Nu	1.25	WRe(25%wt)	13, **	PL:2, BD:4, T(60*)	[32]
TIMET-54M-ATI-425, B	4	WLa-based	~16, F	PL:1.4, BD:N.A., T	[34]

Table 2. Tool geometries used for the FSW of titanium alloys. Dimensions in [mm]. Legend: Butt configuration (B); Base diameter (BD); Cylindrical (Cy); Flat (F); Lap configuration (L); Numerical simulation included (Nu); Pin length (PL); Spherical crown surface (SCS); Tapered (T); Threaded cone (TC); Threaded cylinder (TCy); T-joint configuration (Tj); * Total cone angle; ** No further information is provided.

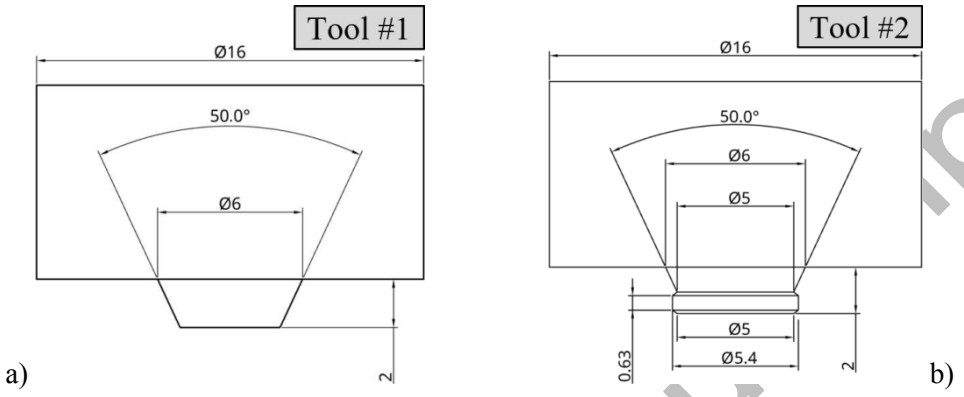

Figure 1. Tool geometries used in the experimental FSW tests: a) truncated conical pin and b) enlarged pin.

Joint configuration	Tilt angle [°]	Plunge depth [mm]	Plunge speed [mm/min]	Dwell time [s]	Rotational speed [rpm]	Welding speed [mm/min]
CP-Ti/CP-Ti	2	2.4	2	3	250	75
Ti6Al4V/Ti6Al4V						
CP-Ti*/Ti6Al4V						
Ti6Al4V*/CP-Ti						

Table 3. Configurations and process parameters for FSW. *Placed as the upper sheet in the lap joint configuration.

During the experimental tests, two sheet coupons (150x100 mm) were overlapped by 50 mm, as shown in Figure 2, firmly fixed with two clamps, and welded in the middle of this region. All the FSW welds were realized using pure argon as the shielding gas at a flow rate of 20 l/min. Two 3 mm diameter nozzles were placed at the front and rear of the FSW tool to protect the weld during the joining process. The titanium coupons were welded at the J-Tech interdepartmental laboratory at the Politecnico di Torino, using a 100 kN FSW machine (mod. FSW100, Stirtec GmbH) with a water-cooled spindle. Figure 3 shows the equipment used to conduct the experimental welding tests. A WC insert was placed in the backplate along the welding line to avoid carbon contamination from the clamping system to the titanium sheets.

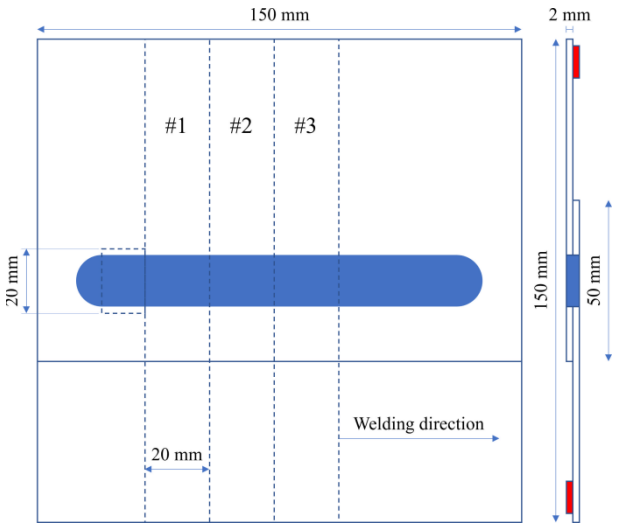

Figure 2. Sketch of the FSW seam and the shear tension sample. The shear tension and the metallographic samples are pointed out by the dotted lines in the welded coupons.

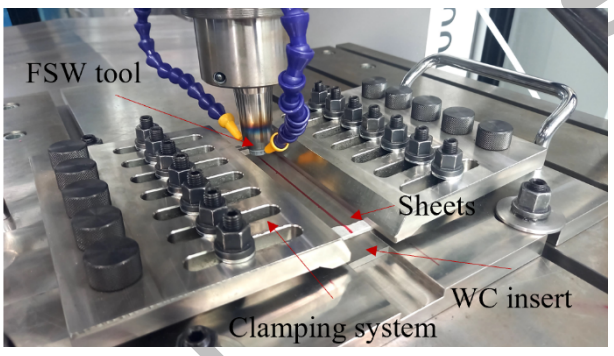

Figure 3. Experimental setup for the FSW tests

Three 20 mm width tensile samples were cut by means of wire electrical discharge machining, and one sample was used for the optical microscopy and the Vickers microhardness measurements, Figure 2. Other specimens were also prepared to obtain consistent results in the mechanical characterization. The strength of the FSW joints was assessed through shear tension tests. The trials were carried out on a standard testing machine with a crosshead speed of 10 mm/min. Shims (the red parts in Figure 2) were applied to the ends of the welded samples to ensure that the center of the joint passed along the same direction as the tensile load. The shear tension strength was evaluated as the peak load reached during the test. The elongation at the peak load was also determined.

The cross-sections of the FSW joints were examined using optical microscopy. The metallographic samples were prepared using a standard procedure, which included grinding, polishing, and a final chemical etching with a Kroll's reagent that confirmed with ASTM E-407 [51]. Vickers microhardness measurements, based on ASTM E92 [52], were conducted to assess the hardness of the microstructures in the cross-section of the joints. A load of 500 g and a holding time of 15 s were selected. An incremental step of 400 µm between two successive indentations was used for the joint cross-sections to measure the microhardness of the stir zone (SZ), the thermo-mechanical affected zone (TMAZ), the heat affected zone (HAZ), and the base metals

(BM). Vickers microhardness maps of the cross-sections of the FSW joints were obtained using a MATLAB suite.

The mechanical strength of the FSW joints was compared with that of similar welds obtained through laser welding (LW). These joints were realized by means of a diode laser source (mod. LDF4000, Optoprim S.r.l.) at the J-Tech interdepartmental laboratory at the Politecnico di Torino. The experimental setup is shown in Figure 4. The coupons to be welded were prepared with the same lap configuration as that adopted for the FSW joints. The following main process parameters were selected for the LW joints: backward torch tilt angle of 10° to the welding direction; laser power of 4.4 kW; welding speed of 25 mm/min. Pure argon was used as the shielding gas. It was fed at a flow rate of 20 l/min through two 3 mm diameter nozzles mounted at the front and at the back of the laser spot to protect the weld seam. The shear tension and metallographic samples were extracted from the laser-welded sheet coupons, as shown in Figure 2. The laser welds were examined with the same procedures adopted for the FSW joints.

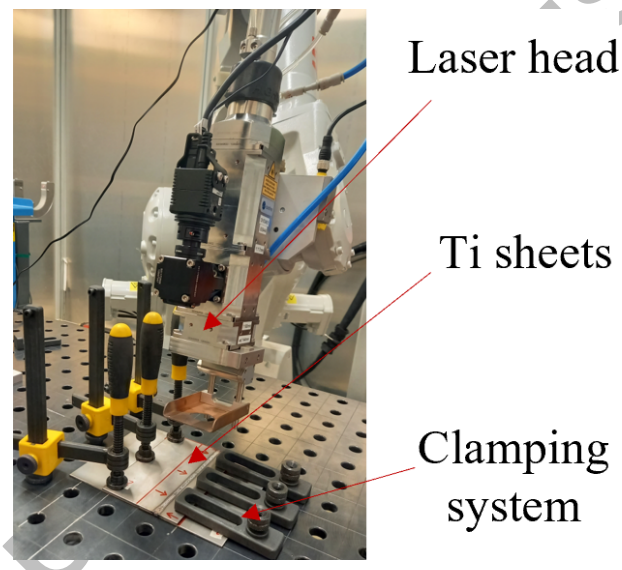

Figure 4. Experimental setup for laser tests.

3. Results and discussion

3.1 FSW process parameters

The spindle torque and vertical force were monitored using specific sensors embedded in the FSW tool head during the joining process. The typical trends of these variable are displayed in Figure 5 for the truncated conical pin tool. The main contribution to spindle torque is caused by the friction and plunging of the tool shoulder against the upper sheet and hence from the mechanical behavior of the upper sheet. When the most resistant Ti6Al4V alloy is placed as the upper sheet, the spindle torque and the forces show the maximum values, since more energy is required to cause friction and stir the Ti alloy with the highest mechanical strength. The spindle torque is almost over 40 Nm (40-47 Nm range) during the welding of the Ti6Al4V/Ti6Al4V joint. Ti6Al4V/CP-Ti requires a lower spindle torque (35-45 Nm range) since the pin penetrates the less resistant lower sheet. Coherently, the spindle torque reduces in the 28-40 Nm range when

the less resistant CP-Ti is placed as the upper sheet. In this case, the spindle torque increases slightly (about 1-2 Nm) when the lower sheet is Ti6Al4V.

The vertical force rapidly increases at the beginning of the plunge phase due to the penetration of the tool pin into the upper sheet. The monitored data show that the vertical force increases much more when Ti6Al4V is placed as the upper sheet, reaching a peak value of about 21 kN. This is due to the higher mechanical strength of Ti6Al4V. More limited values were found when CP-Ti was placed as the upper sheet, with a peak value of about 14 kN. After the peak value, the metal softens, and the force required to proceed with pin plunging is reduced. When the pin touches the lower sheet and the shoulder touches the upper sheet, the vertical force exhibits two different kinds of behavior, which change according to the nature of the lap joint sheets. As seen in Figure 5, the vertical force continues to reduce when Ti6Al4V is the upper sheet, regardless of the nature of the lower sheet. The vertical force instead increases when CP-Ti is the upper sheet. The vertical force reaches a peak value when the shoulder touches the lower sheet and remains almost constant for the rest of the joining process. This behavior could be attributed to the different thermal conductivity of CP-Ti and Ti6Al4V. Ti6Al4V has a thermal conductivity that is more than two times lower than that of CP-Ti (about 7 vs. 17 W/(mK)) [53,54]. When Ti6Al4V is the upper sheet, its lower thermal conductivity maintains heat under the FSW tool, thus promoting a more remarkable softening. A larger amount of heat can also be transferred to the lower sheet promoting its softening. Therefore, a lower force is required to stir the sheets during the joining process. In contrast, when CP-Ti is the upper sheet, its higher thermal conductivity favors a more substantial heat loss that reduces the capability of the upper and lower sheets to raise their temperature and soften. As a result, a higher vertical force is required when CP-Ti is the upper sheet. During the welding, the force remains nearly constant during the process.

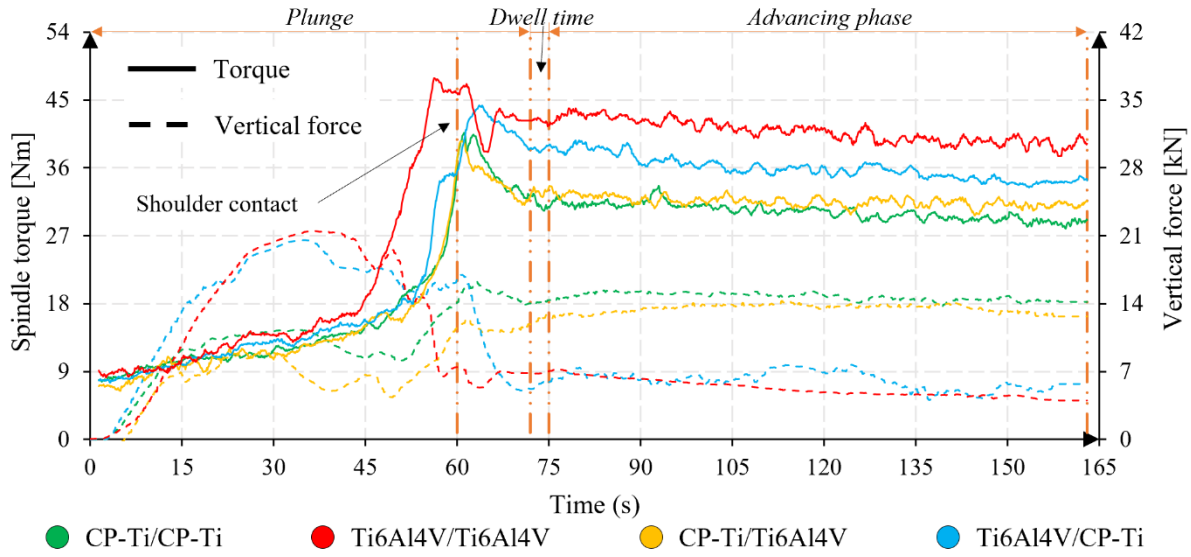

Figure 5. Vertical force and spindle torque involved during the joining of the FSW joints (truncated conical pin tool).

The spindle torque follows the same trend with the enlarged pin tool, Figure 6 a). The spindle torque peak only assumes a lower value (33 kN vs. 40 kN) when the shoulder touches the upper sheet in the dissimilar configuration CP-Ti/Ti6Al4V. The vertical force is instead always higher when using the enlarged pin tool, Figure 6 b). This behavior could be attributed to the flat pin tip that can penetrate the material with more difficulty than the truncated conical shape. Moreover, the vertical force is not almost constant during the advancing phase, but it increases at first and then decreases showing a fork up to 10 kN. This trend is referable to the different shape of the tool, being the welding parameters the same as those used with the truncated conical pin. A possible explanation could be related to the difficulty of high strength-to-mass ratio materials to follow complex tool features and to a consequent instability in the materials flows occurring in the stirred region. Figure 6 c) shows the evidence of a "built up edge'' in the enlarged pin tool at the end of the weld which was not present in the truncated conical pin tool.

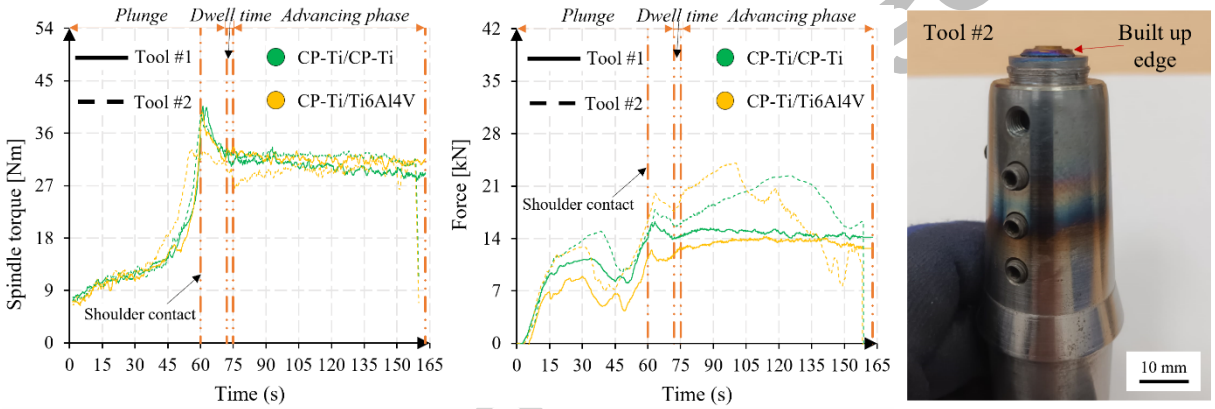

Figure 6. Comparison of the a) spindle torque and b) vertical force monitored with the truncated conical and the enlarged pin tools; c) "built up edge'' in the enlarged pin tool.

The mechanical energy in welding processes can be computed from the spindle torque and rotational speed. The contribution of the vertical force to the energy is negligible (at least three orders of magnitude lower). This energy is only the input energy necessary to join the sheet stack and does not include the energy needed for all the FSW machine subunits and the efficiency of the power chain. Under such assumptions, the energy required to join the sheet stacks is 105 kJ, 107 kJ, 122 kJ, and 140 kJ for the CP-Ti/CP-Ti, CP-Ti/Ti6Al4V, Ti6Al4V/CP-Ti, and Ti6Al4V/Ti6Al4V lap joint configurations, respectively. Due to the stronger material flow, larger energy and spindle torque are required when welding Ti6Al4V.

3.2 Microstructure and hardness examinations

Figures 7 and 8 show the cross-sections of the similar FSW joints obtained with the different tools and the locations of the BM, HAZ, TMAZ, and SZ. The SZ characterizes almost the entire region affected by the process, and its size is coherent with the tool shapes.

Comparing with the truncated conical pin tool, Figure 7 a), the enlarged pin tool, Figure 7 b), involves a larger amount of metal in mixing the two sheets. Therefore, the resulting interface is broader than the one

obtained with the truncated pin tool (6.0 mm vs 4.8 mm). Similarly, the overall SZ is broader as well (21 mm^2 vs 16 mm^2). Figure 8 shows the cross-section of a similar Ti6Al4V joint obtained with the truncated conical pin tool. In this case, the SZ and the interface are notably larger than the ones obtained when CP-Ti is placed as the upper sheet: 24 mm^2 vs 16 mm^2 and 5.6 mm vs 4.8 mm, respectively. Since Ti6Al4V is more resistant than CP-Ti, this effect is attributable to the different thermal conductivity of the two alloys. As described previously, the lower thermal conductivity of Ti6Al4V maintains heat under the FSW tool, thus promoting a more remarkable softening and mixing at this side of the joint. The higher mechanical resistance of Ti6Al4V and the more significant amount of the stirred materials are considered the main factors responsible for the higher torque required when joining the Ti6Al4V/Ti6Al4V and Ti6Al4V/CP-Ti joints. Figures 9 and 10 show the dissimilar joints between CP-Ti and Ti6Al4V alloys obtained with the truncated conical and enlarged pin tools. An increase of the interface from 4.8 mm to 5.8 mm is measured for the CP-Ti/Ti6Al4V joint when using the enlarged pin tool respect to the truncated conical pin tool. Similarly, an increase in the extent of the SZ is found going from 16 mm^2 to 20 mm^2. The cross-section shown in Figure 9 b) confirms that the SZ is broader when Ti6Al4V is placed as the upper sheet: 25 mm^2 and 6.1 mm are evaluated respectively for the SZ area and the lap interface.

Figure 7. Cross-section of CP-Ti/CP-Ti joints with a a) truncated conical pin and b) enlarged pin tool. The colored marks highlight the locations of the microstructures reported in Figure 11.

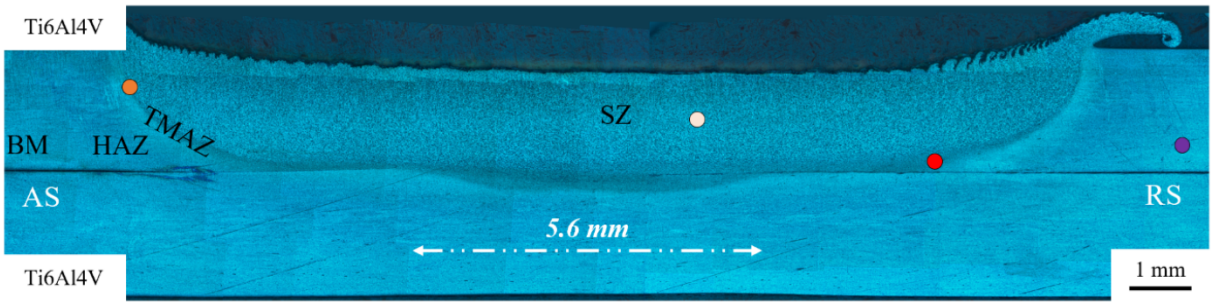

Figure 8. Cross-section of Ti6Al4V/Ti6Al4V FSW joint obtained with a truncated conical pin tool. The colored marks highlight the locations of the microstructures reported in Figure 11.

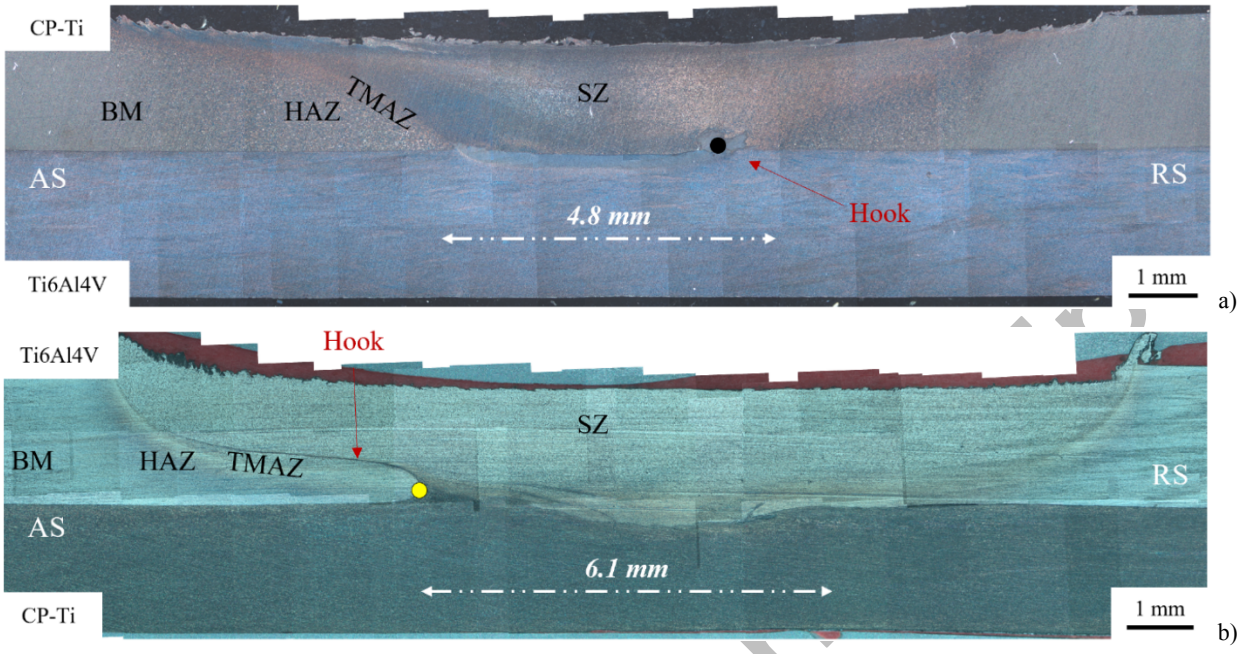

Figure 9. Cross-section of a) CP-Ti/Ti6Al4V and b) Ti6Al4V/CP-Ti FSW joints (truncated conical pin tool). The colored marks highlight the locations of the microstructures reported in Figure 11.

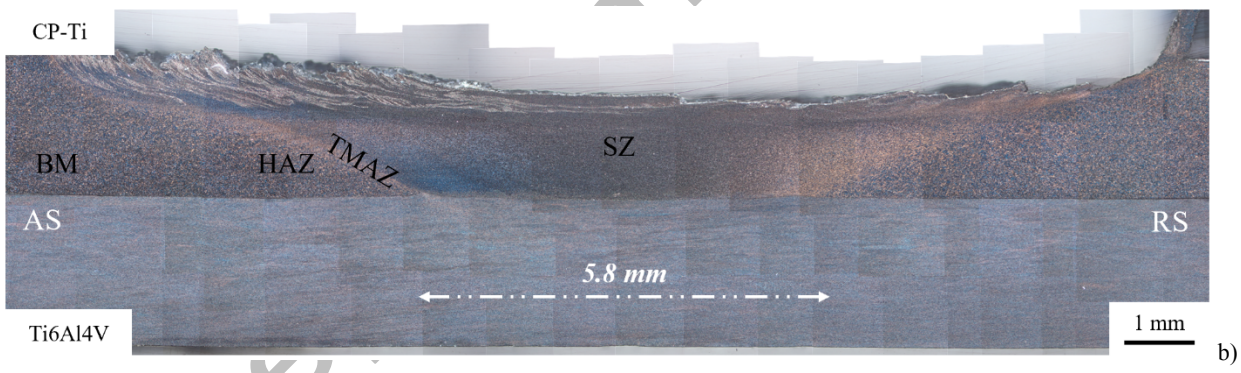

Figure 10. Cross-section of the dissimilar CP-Ti/Ti6Al4V joints obtained with the enlarged pin tool.

Figure 11 shows the microstructures of some characteristic areas in the FSW joints. The average grain size in the CP-Ti/CP-Ti joints moves from 10-15 μm in the BM to about 5-10 μm in the SZ. The average grain size in the Ti6Al4V/Ti6Al4V joints is about 10 μm for the α phase and 5 μm for the β phase in the BM. These values do not considerably change in the SZ proving that FSW does not harm the material microstructure with its heat input. However, the lack of a grain size reduction (as happens for the CP-Ti/CP-Ti joints) can be attributed to the lower thermal conductivity of Ti6Al4V which maintains heat under the FSW tool and faces the typical recrystallization trend occurring in the SZ. Moreover, some acicular structures can be observed for the Ti6Al4V/Ti6Al4V joints proving that some α grains overcome the β-transus temperature range (from 850 °C to 1020 °C [55]) and go under a martensitic transformation [42]. The cross-sections shown from Figure 7 to Figure 10 highlight that the extents of the TMAZ and HAZ are much more limited than that of

the SZ. They appear as thin regions around the SZ that can not be clearly distinguished. As found in the literature for the FSW of titanium alloys [21,22,24,27,42], this particular feature is due to a combination of some factors that limit the formation of wide TMAZ and HAZ regions: (i) low rotational speeds, (ii) a high strength-to-mass ratio, and (iii) low thermal conductivity. Figure 11 shows the extent of a transition region for the CP-Ti/CP-Ti joints and the Ti6Al4V/Ti6Al4V joints. In the former case, it is not visible a defined thickness for this area. In the latter case, it shows a thickness which is affected from the location in the cross-section: about 40 μm along the lateral area interested from the friction tool, about 100 μm moving towards the region forged below it. These transition regions do not show acicular structures meaning that they do not experience temperatures above the β-transus. Finally, the two friction tools employed in this study do not heavily change the microstructure, but their action is mostly related to the increase of the lap interface.

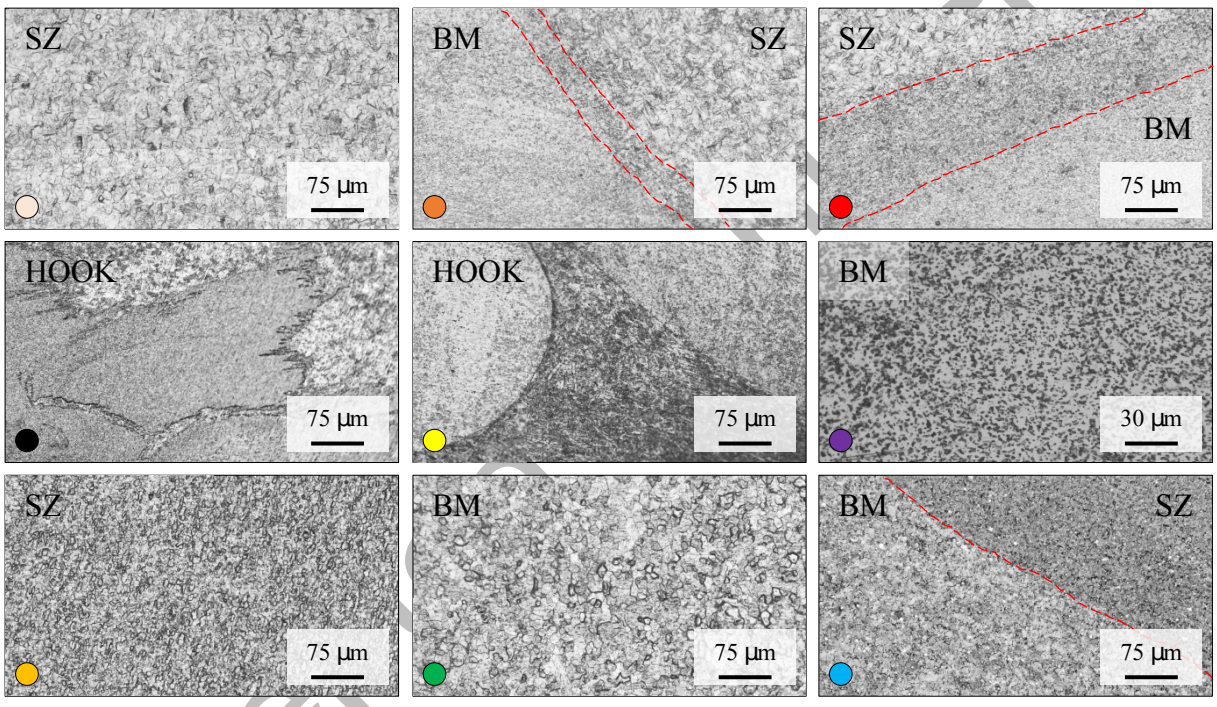

Figure 11. Microstructures of some characteristic areas in the FSW joints.

Some FSW joints obtained with the truncated tool pin show some hook defects (e.g., Figure 9 and Figure 11). These defects are instead absent when welding the joints with the enlarged pin tool. Figure 12 shows a schematic of the different material flows with Tool #1 and Tool #2. Two views are represented: (i) plane perpendicular to the welding direction captured from the leading side (LS) point of view and (ii) plane parallel to the welding direction captured from the AS point of view. Ji and Li [27] summarized the material flows that occur in the FSW of lap titanium joints with a conventional tool. During welding, the material flow moves through the shoulder- and pin-affected zone (SAZ and PAZ, respectively) down to the pin tip and is then concentrated at its bottom. This zone gradually enlarges and moves the material of the adjacent TMAZ by means of an upward flow (UF). Therefore, the original lap interface shows an upward bending morphology which remains as a hook in the joint. A hook can form either in the AS or RS, but it shows a different morphology because the UF meets in the SAZ a discordant flow in the AS and a concordant flow in

RS (see Figure 12). Therefore, the hooks in the RS side are oriented toward the tool rotation axis, while they are confined to the TMAZ in the AS side. These hooks morphologies are slightly visible in Figure 7 a) and Figure 8.

When FSW lap joints between different materials are addressed, their different mechanical properties play a significant role. As seen in Figure 9 a), the hook is more pronounced in the RS for CP-Ti/Ti6Al4V, while it is much thinner in the AS for Ti6Al4V/CP-Ti, Figure 9 b). Ti6Al4V can rise and penetrate the softer CP-Ti in the CP-Ti/Ti6Al4V joint, but the extent of the hook defect within the upper sheet is more limited because of the higher difficulty of the UF to stir the most resistant Ti6Al4V. Differently, the less resistant CP-Ti cannot easily penetrate the more resistant Ti6Al4V alloy in the Ti6Al4V/CP-Ti joint. In this case, only a thin amount of material can move upward within the Ti6Al4V due to the higher deformability of CP-Ti.

As far as the enlarged pin tool is concerned, the cylindrical feature of the pin tip slows the downward flow present in the PAZ. Moreover, the UF contours the larger diameter of the pin and then directly collide with the downward flow producing a more vigorous material stirring. For sake of clarity, Figure 12 compare the SZ produced with the truncated conical pin tool (light grey) with that generated with the enlarged pin tool (dark grey), both drawn from the cross-section of the CP-Ti/CP-Ti joints, Figure 7. The evidence of a “built up edge” in Figure 6 c) suggests an instability in the material flows occurring in the stirred region which was reported in Figure 12. This phenomenon could be caused by a constriction of the extrusion zone due to the presence of the enlarged pin tip. Moreover, it can be macroscopically related to the not constant vertical force, as shown in Figure 6 b). Therefore, the solution found from Huang et al. [38,39] for Al/Al and Al/steel lap joints should be customized for titanium lap welds due to the difficulty of high strength-to-mass ratio materials to follow complex tool features.

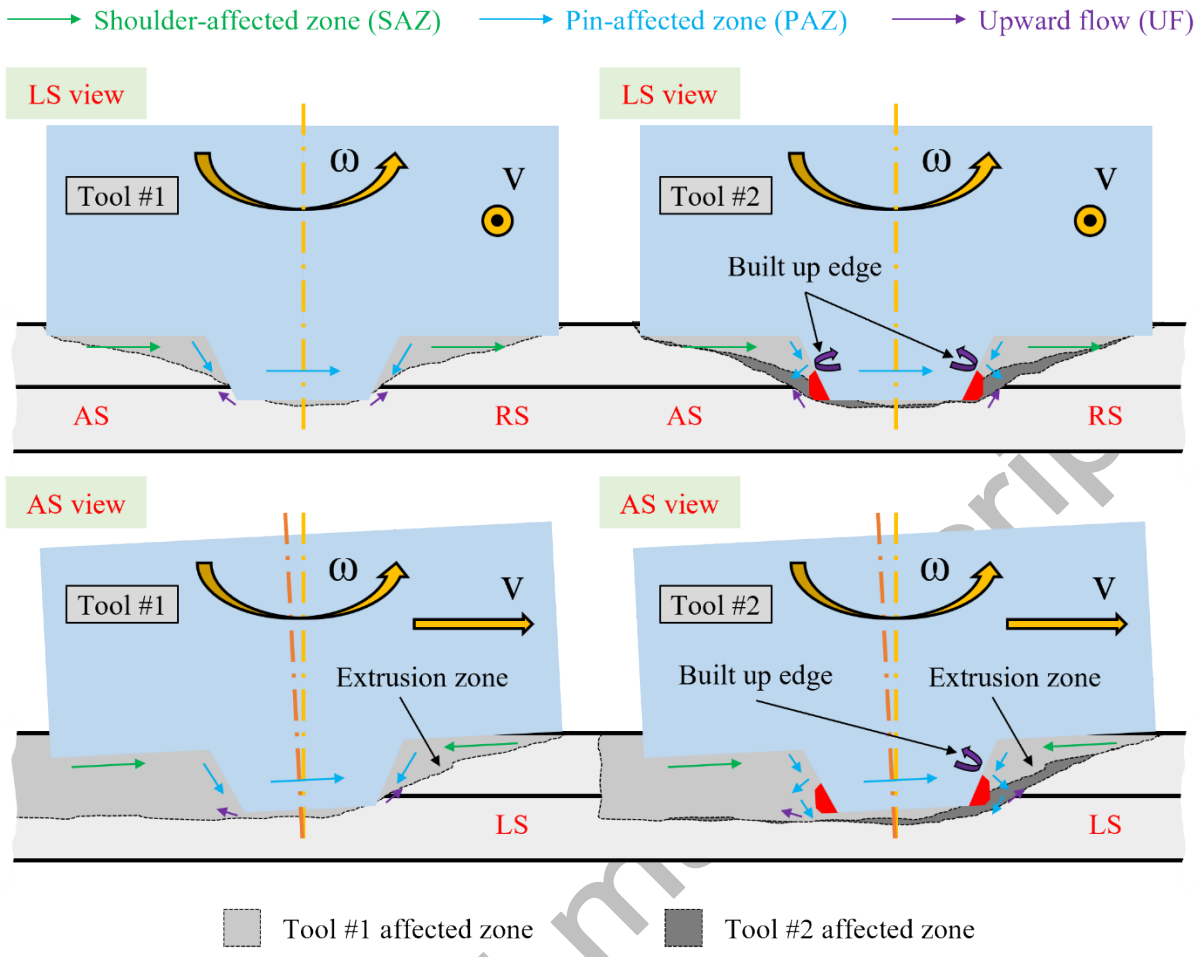

Figure 12. Schematic of the different material flows with Tool #1 and Tool #2: view plane perpendicular to the welding direction (from the LS point of view) and view plane parallel to the welding direction (from the AS point of view). The SZ regions were drawn from the cross-section of the CP-Ti/CP-Ti joints.

Figure 13 compares the hardness maps of the cross-sections of the CP-Ti/CP-Ti and Ti6Al4V/Ti6Al4V joints. The hardness distribution does not change using the different tools. The FSW joints realized with the enlarged pin only show broader joints accordingly to the tool shape. The hardness reaches a peak value in the SZ and then reduces moving toward the BM. This hardness ranges from 280 to 220 HV0.5 for the CP-Ti/CP-Ti joint, while it changes from 360 to 340 HV0.5 for the Ti6Al4V/Ti6Al4V joint. The more significant increase in hardness of CP-Ti is associated with its higher strain hardening capability (strain hardening exponent of about 0.20 [56]) than that of Ti6Al4V (strain hardening exponent of about 0.05 [57]). The dissimilar joints show a similar hardness distribution with intermediate hardness values from the SZ toward the BM.

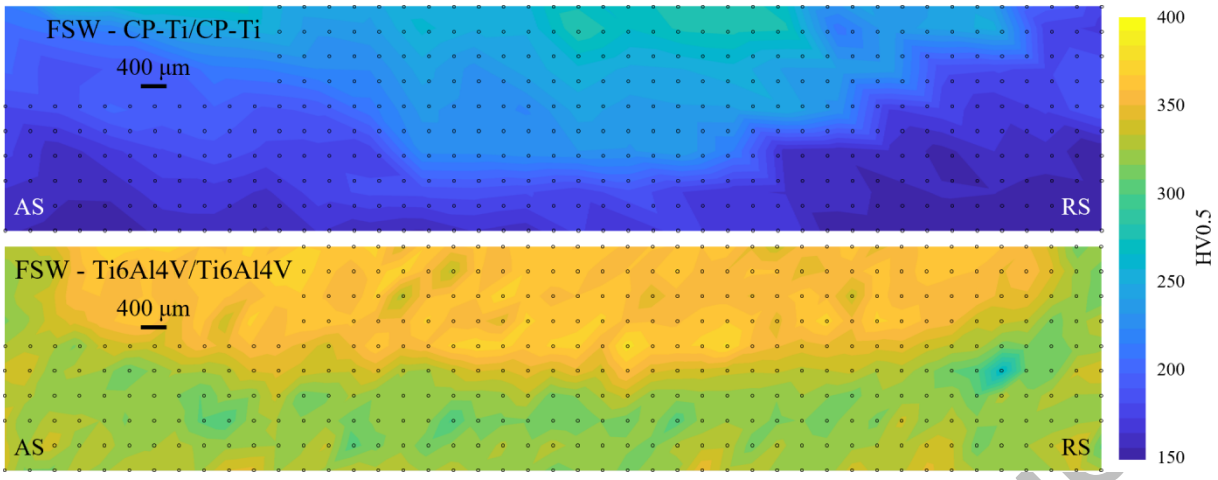

Figure 13. Vickers microhardness map of similar FSW joints (truncated conical pin tool). Each black dot is a microhardness indentation.

3.3 LW joints

Figure 14 shows a cross-section of the laser-welded CP-Ti/Ti6Al4V and Ti6Al4V/CP-Ti joints and the corresponding extent of the BM, HAZ, and fused zone (FZ). As reported in Oliveira et al. [58,59], LW can be carried out in conduction mode or in keyhole mode. A method of distinction between these two welding modes consists in the evaluation of the aspect ratio (width/depth ratio). Conduction mode occurs if it is significantly larger than unity. Figure 14 shows that a mixed conduction + keyhole mode is experienced from both joints. It ranges from about 0.25 for the lower plate to about 0.95 for the upper one. This geometry results from the relative slow welding speed which is necessary to achieve an adequate depth in the joint. The chemical etching reveals a different grain size distribution for the two joints, which is due to the different chemical compositions of the two alloys and to the mixed conduction + keyhole welding mode. The CP-Ti/Ti6Al4V joint shows an uneven grain size in the FZ throughout the thickness of the joints. The grain size ranges from 250 to 30 µm when moving from the upper sheet (CP-Ti) to the lower one (Ti6Al4V). This distribution is due to the different cooling times of the molten pool. For instance, columnar grains can be observed in the upper plate because of the metal solidifying more slowly since it faces the laser beam. More globular and smaller grains can be observed in the internal area of the lower sheet, while larger grains are still observed in its HAZ because the heat flux towards the BM promotes the growth of the grains instead of their nucleation [58]. A finer grain size, in the 15-30 µm range, was measured in the FZ of the Ti6Al4V/CP-Ti joint. The smaller grain size can be attributed to the nucleation effect of the chemical elements of Ti6Al4V. This is coherent with the stronger nucleation effect of the segregated elements in the last portions of the molten pool, which makes the grains finer in the center of the weld. An improvement of the LW joints can be achieved if a keyhole welding mode is carried out, as reported in Oliveira et al. [59] for high-strength metals.

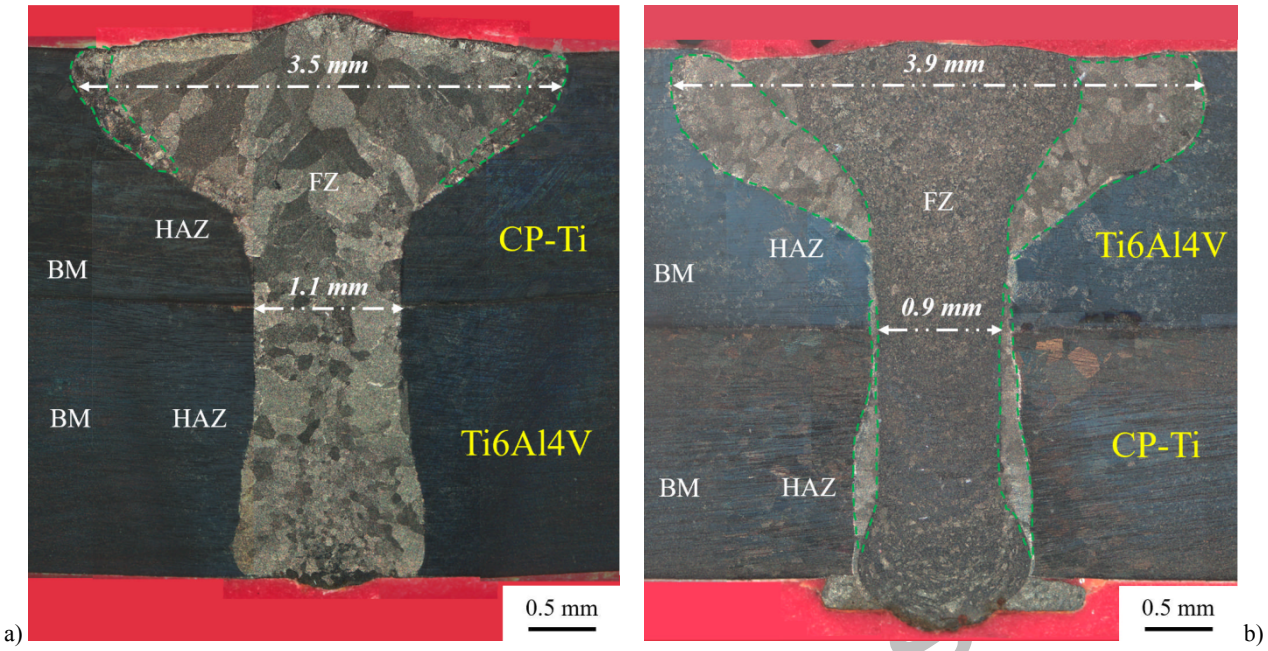

Figure 14. Cross-section of a) CP-Ti/Ti6Al4V and b) Ti6Al4V/CP-Ti LW joints.

3.4 Joint shear tension strength

Figure 15 a) shows the results of the shear tests performed on the titanium sheets (CP-Ti, Ti6Al4V), FSW and LW joints, while Figure 15 b) shows their tensile test curves. As expected, Ti6Al4V exhibits an average strength of 44 kN, while CP-Ti has a more limited strength of 18 kN. The FSW Ti6Al4V/Ti6Al4V joint shows the most resistant strength of 29 kN, which is about 38 % lower than that of the base metal. The CP-Ti/CP-Ti and dissimilar joints exhibit a strength, about 17-19 kN, like that of CP-Ti, and 63 % lower than that of Ti6Al4V. As discussed hereafter when examining the fracture locations, CP-Ti mainly drives the mechanical performances of these joints. The elongation at the peak load values highlights the low ductility of the examined joints compared to the base metals. The CP-Ti and the Ti6Al4V samples have a similar elongation for the peak load, that is, of about 10-11 mm. The FSW samples range from about 6 to 8.5 mm, with the minimum value being obtained for the most resistant Ti6Al4V/Ti6Al4V joint and the maximum value being obtained for the CP-Ti/CP-Ti joint (8 mm), due to the higher ductility of the CP-Ti alloy. The dissimilar FSW joints show intermediate values (6.5-7.5 mm).

The enlarged pin tool has a slight effect on improving the mechanical strength of the joints, but it gives the same rigidity of the Ti6Al4V BM due to the higher lap interface, see Figure 15 b). It slightly improves the elongation at fracture of the similar joint, while its effect is more pronounced for the dissimilar weld (6.5 % vs. 10 %) because it was more severely affected from the hook defect. However, these welds are characterized from a higher variability due to the not constant vertical force, which in turn is caused from the instability in the material flows occurring in the SZ.

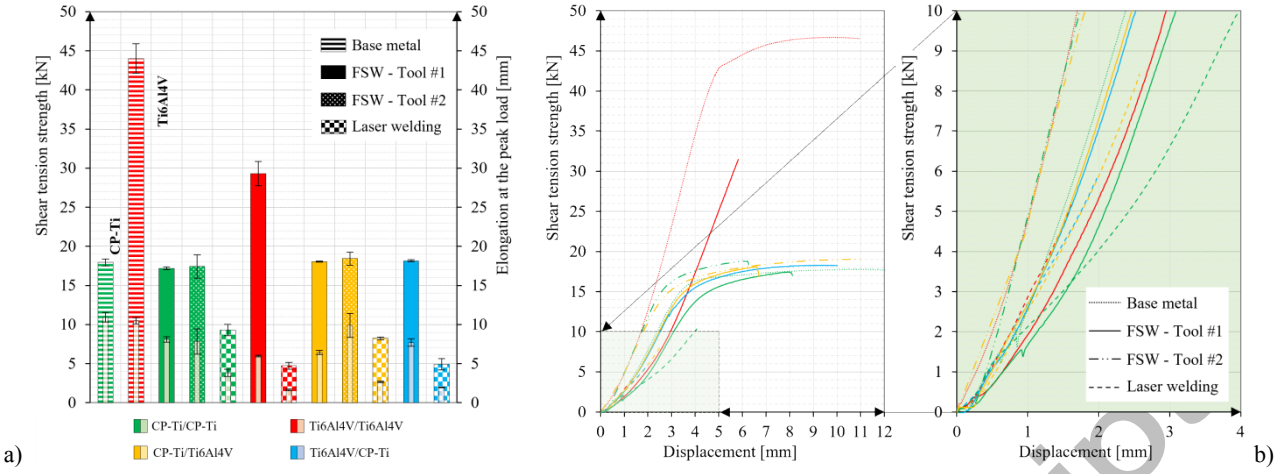

Figure 15. Results of the shear tension tests performed on the FSW and LW joints: a) mean values and standard deviations of the shear tension strength (left-hand scale) and the elongation at the peak load (right-hand scale) and b) tensile test curves.

Figures 16, 17, 18, and 19 show the fracture paths of the similar and dissimilar FSW joints. All the joints failed with similar behavior using the truncated conical and enlarged pin tools, that is, with the crack nucleating in the unwelded region at the interface of the two sheets surrounding the FSW joint. This is a typical type of fracture of FSW lap joints because this location acts as a notch when the joints are under stress. The rupture in the CP-Ti/CP-Ti joints propagated through the SZ toward the upper surface. Although the SZ was more resistant than the other joint regions, the crack propagated in this region due to the smaller resistant cross-section resulting from the squeezing of the tool shoulder. In some cases, a slight necking is visible at the fracture end of the joint, Figure 16 a) and b). Guan et al. [45] and Ma et al. [46] have proposed new tool shapes with an inner and outer shoulder to eliminate flash and weld thinning in FSW of 6xxx and 2xxx aluminum alloys. During welding, the metal around the pin flowed downwards, and those away from the pin flowed upwards. The outer shoulder prevents plasticized materials from flowing out and refilling them into the joint. This solution could also be adopted for titanium alloys, but further comprehensive studies are necessary to investigate the influence of the tool geometry on reducing thinning and flash in such high-strength alloys.

The fracture mode differed in the other similar Ti6Al4V/Ti6Al4V joints since the fracture propagated through the lower sheet, Figure 17. Despite the more limited cross-section of the SZ, the greater hardness prevented the propagation of the crack across this region. No signs of local necking were observed. The fracture in the CP-Ti/Ti6Al4V joints nucleated in the hook region on the RS side and then propagated in the SZ toward the upper surface, Figure 18 a). In this case, the lower strength CP-Ti as the upper sheet also promoted failure of the joints in this region. The hook has promoted the crack nucleation and propagation in the RS side instead of the AS, as it instead occurs for the other FSW joints. The same joint configuration without the hook, which was obtained with the enlarged pin tool, failed in the AS, Figure 18 b). The fracture of the Ti6Al4V/CP-Ti joints, Figure 19, occurred through the Ti6Al4V upper sheet. This results from the crack nucleation and the following propagation along the long hook defect made by the less resistant CP-Ti

material, which penetrated the most resistant upper sheet. Therefore, the hook defect promotes the crack propagation through the stronger Ti6Al4V instead of in the softer CP-Ti, as occurs in all the other joints.

Liu et al. [21,23] found lower shear tension strength values, 14.5 kN, during lap welding of 2 mm thick CP-Ti sheets. The joints failed in the BM. Ji and Li [27] obtained a strength of 17 kN for Ti6Al4V/Ti6Al4V lap joints (1.8 mm thick sheet and 20 mm wide specimen). They reported that the crack nucleated in a hook defect in the AS and then propagated across the SZ. The study of Buffa et al. [28], conducted on Ti6Al4V/Ti6Al4V lap joints (1.2 mm thick sheets), showed a joint strength from 350-750 MPa for varying process parameters, with the failure always occurring in the bottom sheet at the AS.

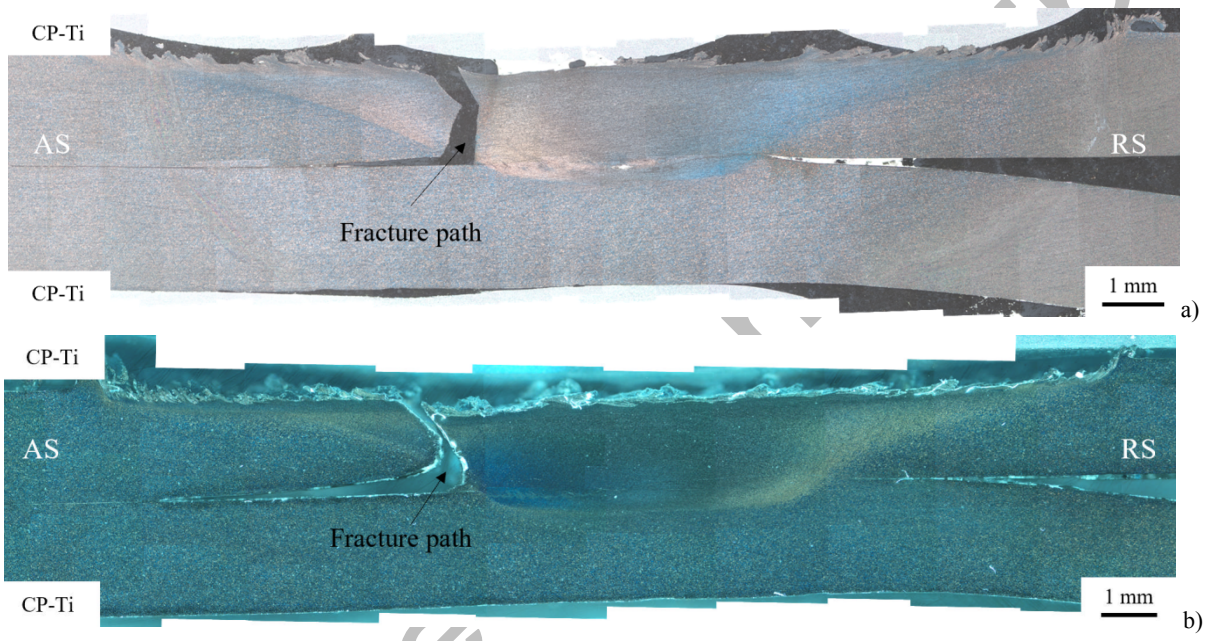

Figure 16. Cross-section of a failed CP-Ti/CP-Ti FSW joints obtained with the a) truncated conical and b) enlarged pin tools.

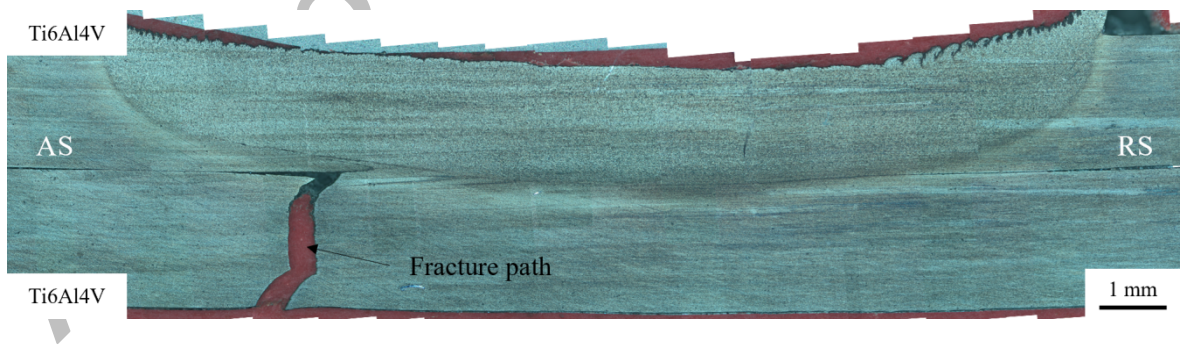

Figure 17. Cross-section of a failed Ti6Al4V/Ti6Al4V FSW joint obtained with the truncated conical pin tool.

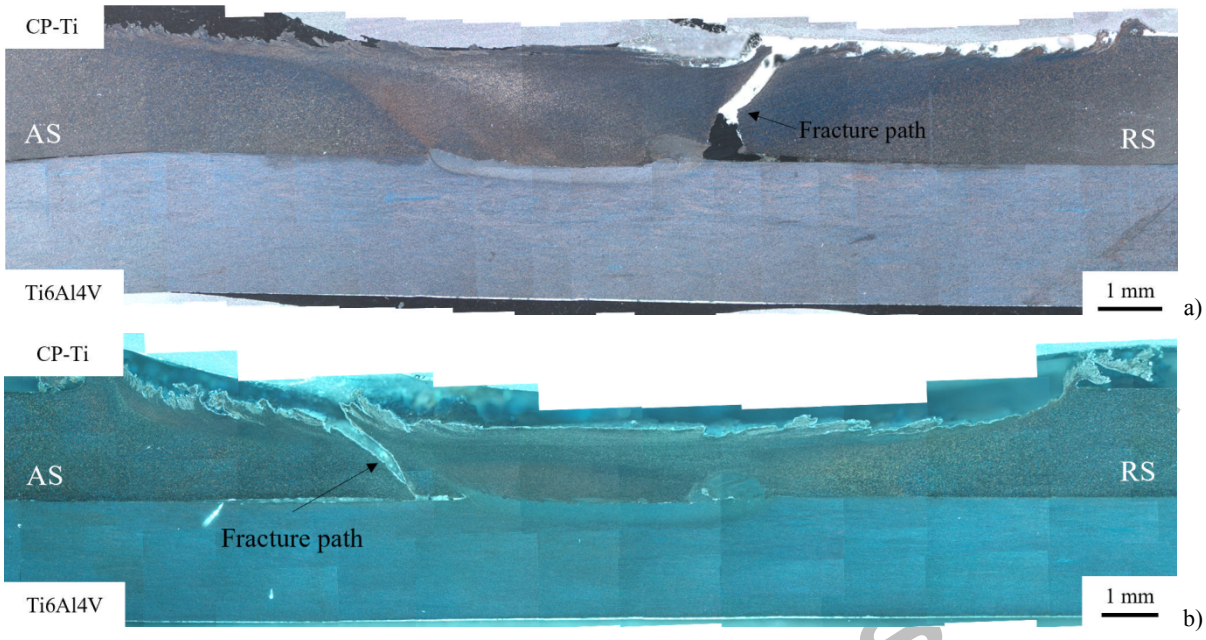

Figure 18. Cross-section of a failed CP-Ti/Ti6Al4V FSW joints obtained with the a) truncated conical and b) enlarged pin tools.

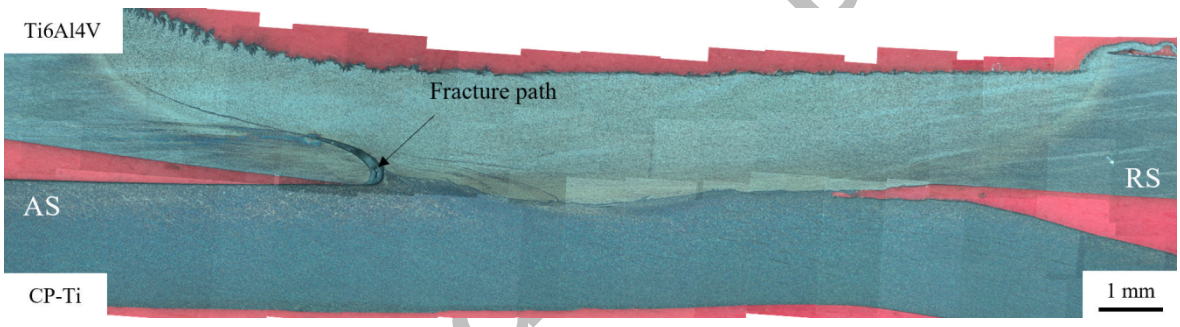

Figure 19. Cross-section of a failed Ti6Al4V/CP-Ti FSW joint obtained with the truncated conical pin tool.

The magnification shown in Figure 15 b) highlights that the LW joints have the worst shear tension strength. Overall, the shear tension strength of these joints reduces by about -45 %, -85 %, -55 %, and -75 % for the CP-Ti/CP-Ti, Ti6Al4V/Ti6Al4V, CP-Ti/Ti6Al4V, and Ti6Al4V/CP-Ti joints, respectively (Figure 20). This somewhat limited shear tension strength is due to the harmful effect of fusion welding on the joint microstructures of the Ti alloys. The Ti6Al4V similar and dissimilar joints show the most marked strength reductions because of the formation of large amounts of the brittle β phase in the weldments. Regardless of its position, the dissimilar laser joints always failed in Ti6Al4V alloy. A brittle appearance characterizes the fracture surfaces of the Ti6Al4V/Ti6Al4V and Ti6Al4V/CP-Ti joints, but with no apparent signs of ductility (i.e., no local deformation). The CP-Ti/CP-Ti and CP-Ti/Ti6Al4V joints showed slightly better ductility, even though the elongation of these samples remained at least two times less than that of the corresponding FSW joints.

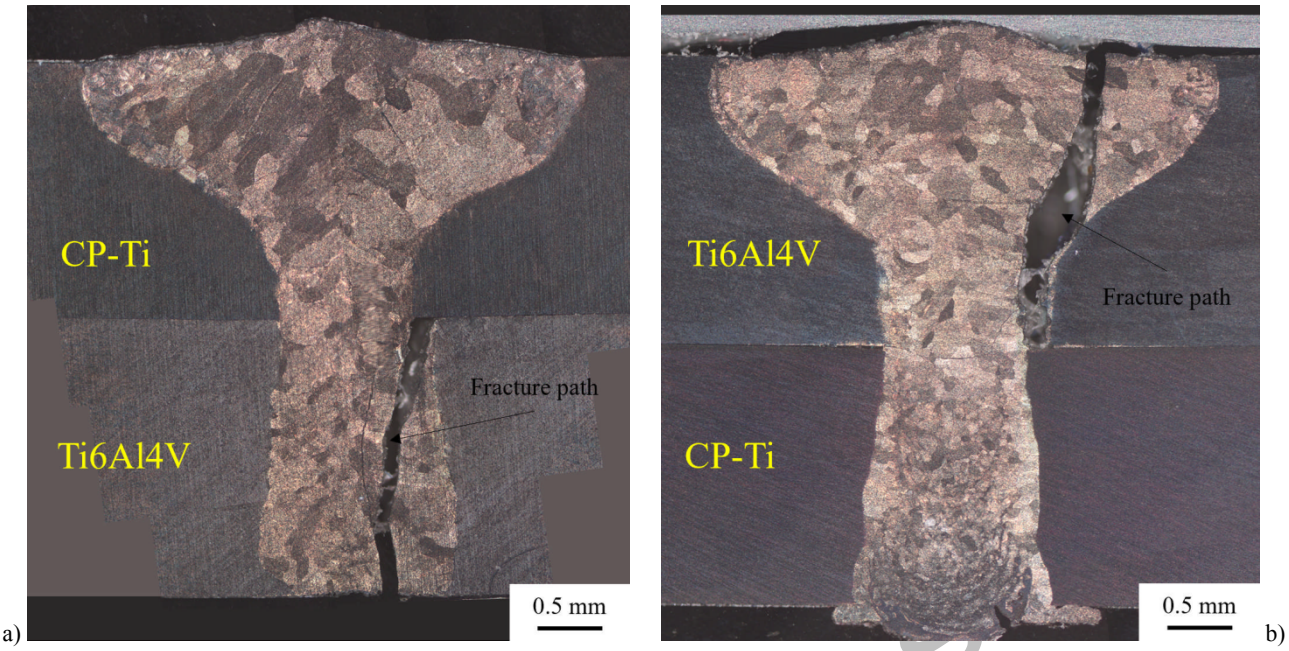

Figure 20. Cross-section of the failed a) CP-Ti/Ti6Al4V and b) Ti6Al4V/CP-Ti joints obtained by laser welding.

4. Conclusions

The main findings of this work are summarized hereafter:

- The spindle torque and vertical force were successfully related to the welding practice to each joint configuration. They showed that the spindle torque and vertical force are related to the upper sheet strength and thermal conductivity. During the welding phase, the vertical force shows a regular trend when using the truncated pin tool. Contrary, it reports a large variability (from 10 kN to 23 kN) with the enlarged pin tool.

- Hook defects clearly appear in the dissimilar FSW joints when the truncated pin tool is used. Hook defects can show a different shape based on the different mechanical properties of the Ti sheets. CP-Ti/Ti6Al4V joints show wider and short hook defects in the RS, while they appear as a thin line in the AS of Ti6Al4V/CP-Ti welds. The cylindrical feature of the enlarged pin tip slows the downward flow present in the PAZ. Moreover, the UF contours the larger diameter of the pin and then directly collide with the downward flow producing a more vigorous material stirring which eliminates hooks. With the enlarged pin tool, the "built up edge" phenomenon suggests an instability in the material flows occurring in the stirred region. This phenomenon could be caused by a constriction of the extrusion zone due to the presence of the enlarged pin tip.

- The Ti6Al4V/Ti6Al4V joints exhibited the highest mechanical strength, about 29 kN, against 44 kN of the BM. Similar and dissimilar CP-Ti joints showed a strength like the base metal, about 17-18 kN, but 63 % less than Ti6Al4V. The elongation at the peak load of the FSW joints was also lower than those of the Ti BMs. The enlarged pin tool has a superior effect on improving the elongation at fracture of the dissimilar weld (6.5 % vs. 10 %) respect to the similar one, because it was more severely affected from the hook defect. However, these welds are characterized from a higher variability due to the not constant vertical force, which in turn is caused from the instability in the material flows occurring in the SZ.

- The laser-welded joints have shown a mechanical strength at least 50 % lower than the corresponding FSW joints. The formation of brittle phases during the solidification of the laser-welded joints, which instead do not form in solid-state joining, is responsible for this significant reduction in strength.

The fundings of this work suggest the necessity to customize welding tools devoted to the elimination of the hook defect due to the difficulty of high strength-to-mass ratio materials to follow complex tool features.

Statements and Declarations

a. Funding This study was supported by J-Tech@PoliTO, an advanced joining technologies research center at Politecnico di Torino (http://www.j-tech.polito.it/) **b. Conflicts of interest/Competing interests** The authors declare no conflicts of interest or competing interests **c. Availability of data and material** All data generated or analyzed during this study are included within the article **d. Code availability** Not applicable **e. Ethics approval** Compliance with ethical standards **f. Consent to participate** All authors agreed with the consent to participate **g. Consent for publication** All authors have read and agreed to the publication of the paper.

References

[1] Callegari B, Oliveira JP, Aristizabal K, Coelho RS, Brito PP, Wu L, et al. In-situ synchrotron radiation study of the aging response of Ti-6Al-4V alloy with different starting microstructures. Mater Charact 2020;165:110400. https://doi.org/10.1016/j.matchar.2020.110400.

[2] Callegari B, Oliveira JP, Coelho RS, Brito PP, Schell N, Soldera FA, et al. New insights into the microstructural evolution of Ti-5Al-5Mo-5V-3Cr alloy during hot working. Mater Charact 2020;162:110180. https://doi.org/10.1016/j.matchar.2020.110180.

[3] Salvador CAF, Maia EL, Costa FH, Escobar JD, Oliveira JP. A compilation of experimental data on the mechanical properties and microstructural features of Ti-alloys. Sci Data 2022;9:188. https://doi.org/10.1038/s41597-022-01283-9.

[4] Cui C, Hu B, Zhao L, Liu S. Titanium alloy production technology, market prospects and industry development. Mater Des 2011;32:1684–91. https://doi.org/10.1016/j.matdes.2010.09.011.

[5] Ke WC, Oliveira JP, Ao SS, Teshome FB, Chen L, Peng B, et al. Thermal process and material flow during dissimilar double-sided friction stir spot welding of AZ31/ZK60 magnesium alloys. J Mater Res Technol 2022;17:1942–54. https://doi.org/10.1016/j.jmrt.2022.01.097.

[6] Oliveira JP, Duarte JF, Inácio P, Schell N, Miranda RM, Santos TG. Production of Al/NiTi composites by friction stir welding assisted by electrical current. Mater Des 2017;113:311–8. https://doi.org/10.1016/j.matdes.2016.10.038.

[7] Costa AMS, Oliveira JP, Pereira VF, Nunes CA, Ramirez AJ, Tschiptschin AP. Ni-based Mar-M247 superalloy as a friction stir processing tool. J Mater Process Technol 2018;262:605–14. https://doi.org/10.1016/j.jmatprotec.2018.07.034.

[8] Mehdi B, Badji R, Ji V, Allili B, Bradai D, Deschaux-Beaume F, et al. Microstructure and residual stresses in Ti-6Al-4V alloy pulsed and unpulsed TIG welds. J Mater Process Technol 2016;231:441–8. https://doi.org/10.1016/j.jmatprotec.2016.01.018.

[9] Edwards P, Ramulu M. Surface Residual Stresses in Ti-6Al-4V Friction Stir Welds: Pre- and Post-Thermal Stress Relief. J Mater Eng Perform 2015;24:3263–70. https://doi.org/10.1007/s11665-015-1610-2.

[10] Su Y, Li W, Liu X, Gao F, Yu Y, Vairis A. Strengthening mechanism of friction stir welded alpha titanium alloy specially designed T-joints. J Manuf Process 2020;55:1–12. https://doi.org/10.1016/j.jmapro.2020.03.032.

[11] Shrivastava A, Krones M, Pfefferkorn FE. Comparison of energy consumption and environmental impact of friction stir welding and gas metal arc welding for aluminum. CIRP J Manuf Sci Technol 2015;9:159–68. https://doi.org/10.1016/j.cirpj.2014.10.001.

[12] Mishra RS, Ma ZY. Friction stir welding and processing. Mater Sci Eng R Reports 2005;50:1–78. https://doi.org/10.1016/j.mser.2005.07.001.

[13] Meng X, Huang Y, Cao J, Shen J, Jorge F. Recent progress on control strategies for inherent issues in friction stir welding. Prog Mater Sci 2021;115:100706. https://doi.org/https://doi.org/10.1016/j.pmatsci.2020.100706.

[14] Mironov S, Sato YS, Kokawa H. Friction-stir welding and processing of Ti-6Al-4V titanium alloy: A review. J Mater Sci Technol 2018;34:58–72. https://doi.org/10.1016/j.jmst.2017.10.018.

[15] Sesha KSN, Yamanaka K, Mori M, Onuki Y, Sato S, Fabrègue D, et al. Demonstrating a duplex TRIP/TWIP titanium alloy via the introduction of metastable retained β-phase. Mater Res Lett 2022;10:754–61. https://doi.org/10.1080/21663831.2022.2096419.

[16] Qiu G, Guo Y. Current situation and development trend of titanium metal industry in China. Int J Miner Metall Mater 2022;29:599–610. https://doi.org/10.1007/s12613-022-2455-y.

[17] Division of Banner Industries. Supra Alloys. Last time accessed on August 31 2022 n.d. http://www.supraalloys.com/titanium-grades.php.

[18] Lunetto V, Priarone PC, Kara S, Settineri L. A comparative LCA method for environmentally friendly manufacturing: Additive manufacturing versus Machining case. Procedia CIRP, vol. 98, 2021, p. 406–11. https://doi.org/10.1016/j.procir.2021.01.125.

[19] Lunetto V, Catalano AR, Priarone PC, Salmi A, Atzeni E, Moos S, et al. Additive manufacturing for an urban vehicle prototype: re-design and sustainability implications. Procedia CIRP 2021;99:364–9. https://doi.org/10.1016/j.procir.2021.03.104.

[20] Reshad Seighalani K, Besharati Givi MK, Nasiri AM, Bahemmat P. Investigations on the Effects of the Tool Material, Geometry, and Tilt Angle on Friction Stir Welding of Pure Titanium. J Mater Eng Perform 2010;19:955–62. https://doi.org/10.1007/s11665-009-9582-8.

[21] Liu H, Nakata K, Yamamoto N, Liao J. Friction stir welding of pure titanium lap joint. Sci Technol Weld Join 2010;15:428–32. https://doi.org/10.1179/136217110X12731414740031.

[22] Liu H, Nakata K, Yamamoto N, Liao J. Grain Orientation and Texture Evolution in Pure Titanium Lap Joint Produced by Friction Stir Welding. Mater Trans 2010;51:2063–8. https://doi.org/10.2320/matertrans.M2010242.

[23] Liu FC, Liu H, Nakata K, Yamamoto N, Liao J. Investigation on friction stir welding parameter design for lap joining of pure titanium. Proc. 1st Int. Jt. Symp. Join. Weld., Elsevier; 2013, p. 159–63. https://doi.org/10.1533/978-1-78242-164-1.159.

[24] Zhang Y, Sato YS, Kokawa H, Park SHC, Hirano S. Stir zone microstructure of commercial purity titanium friction stir welded using pcBN tool. Mater Sci Eng A 2008;488:25–30. https://doi.org/10.1016/j.msea.2007.10.062.

[25] Du S, Liu H, Jiang M, Hu Y, Zhou L. Eliminating the cavity defect and improving mechanical properties of TA5 alloy joint by titanium alloy supporting friction stir welding. J Manuf Process 2021;69:215–22. https://doi.org/10.1016/j.jmapro.2021.07.044.

[26] Amirov AI, Eliseev AA, Beloborodov VA, Chumaevskii A V., Gurianov DA. Formation of α' titanium welds by friction stir welding. J Phys Conf Ser 2020;1611:012001. https://doi.org/10.1088/1742-6596/1611/1/012001.

[27] Ji S, Li Z. Reducing the Hook Defect of Friction Stir Lap Welded Ti-6Al-4V Alloy by Slightly Penetrating into the Lower Sheet. J Mater Eng Perform 2017;26:921–30. https://doi.org/10.1007/s11665-017-2512-2.

[28] Buffa G, Fratini L, Schneider M, Merklein M. Effect of Process Parameters on the Joint Integrity in Friction Stir Welding of Ti-6Al-4V Lap Joints. Key Eng Mater 2013;554–557:1083–90. https://doi.org/10.4028/www.scientific.net/KEM.554-557.1083.

[29] Zhang Y, Sato YS, Kokawa H, Park SHC, Hirano S. Microstructural characteristics and mechanical properties of Ti–6Al–4V friction stir welds. Mater Sci Eng A 2008;485:448–55. https://doi.org/10.1016/j.msea.2007.08.051.

[30] Edwards P, Ramulu M. Identification of Process Parameters for Friction Stir Welding Ti–6Al–4V. J Eng Mater Technol 2010;132:0310061–03100610. https://doi.org/10.1115/1.4001302.

[31] Edwards PD, Ramulu M. Material flow during friction stir welding of Ti-6Al-4V. J Mater Process Technol 2015;218:107–15. https://doi.org/10.1016/j.jmatprotec.2014.11.046.

[32] Buffa G, Fratini L, Schneider M, Merklein M. Micro and macro mechanical characterization of friction stir welded Ti–6Al–4V lap joints through experiments and numerical simulation. J Mater Process Technol 2013;213:2312–22. https://doi.org/10.1016/j.jmatprotec.2013.07.003.

[33] Buffa G, Ducato A, Fratini L. FEM based prediction of phase transformations during Friction Stir Welding of Ti6Al4V titanium alloy. Mater Sci Eng A 2013;581:56–65. https://doi.org/10.1016/j.msea.2013.06.009.

[34] Gangwar K, Ramulu M, Cantrell A, Sanders D. Microstructure and Mechanical Properties of Friction Stir Welded Dissimilar Titan[1] Gangwar K, Ramulu M, Cantrell A, Sanders D. Microstructure and Mechanical Properties of Friction Stir Welded Dissimilar Titanium Alloys: TIMET-54M and ATI-425. Metals (Ba. Metals (Basel) 2016;6:252. https://doi.org/10.3390/met6100252.

[35] Gonser MJ. Microstructure Evolution and Material Flow Behavior in Friction-Stir Welded Dissimilar Titanium Alloys. The Ohio State University, 2010.

[36] Buhl N, G W, Eifler D, Gutensohn M, Zillekens F. Microstructural and Mechanical Investigations of Friction Stir Welded TI/TI- And TI-Alloy/TI-Alloy-Joints. In: Mishra, R., Mahoney, M.W., Sato, Y., Hovanski, Y., Verma R, editor. Frict. Stir Weld. Proceesing VII, Springer; 2013, p. 141–2. https://doi.org/https://doi.org/10.1007/978-3-319-48108-1_15.

[37] ASTM International. Standard Specification for Titanium and Titanium Alloy Strip, Sheet, and Plate ASTM B265 2020:12. https://doi.org/10.1520/B0265-20A.2.

[38] Huang Y, Wan L, Meng X, Xie Y, Lv Z, Zhou L. Probe shape design for eliminating the defects of friction stir lap welded dissimilar materials. J Manuf Process 2018;35:420–7. https://doi.org/10.1016/j.jmapro.2018.08.026.

[39] Yongxian H, Long W, Xiaoqing S, Tifang H, Xiangchen M, Yuming X. Achieving High-Quality Al/Steel Joint with Ultrastrong Interface. Metall Mater Trans A 2019;50:295–9. https://doi.org/10.1007/s11661-018-5006-4.

[40] Gao F, Guo Y, Qiu S, Yu Y, Yu W. Fracture toughness of friction stir welded TA5 titanium alloy joint. Mater Sci Eng A 2020;776:138962. https://doi.org/10.1016/j.msea.2020.138962.

[41] Gao F, Guo Y, Yang S, Yu Y, Yu W. Fatigue properties of friction stir welded joint of titanium alloy. Mater Sci Eng A 2020;793:139819. https://doi.org/10.1016/j.msea.2020.139819.

[42] Li J, Shen Y, Hou W, Qi Y. Friction stir welding of Ti-6Al-4V alloy: Friction tool, microstructure, and mechanical properties. J Manuf Process 2020;58:344–54. https://doi.org/10.1016/j.jmapro.2020.08.025.

[43] Li J, Cao F, Shen Y. Effect of Welding Parameters on Friction Stir Welded Ti–6Al–4V Joints: Temperature, Microstructure and Mechanical Properties. Metals (Basel) 2020;10:940. https://doi.org/10.3390/met10070940.

[44] Pasta S, Reynolds AP. Residual stress effects on fatigue crack growth in a Ti-6Al-4V friction stir weld. Fatigue Fract Eng Mater Struct 2008;31:569–80. https://doi.org/10.1111/j.1460-2695.2008.01258.x.

[45] Fall A, Monajati H, Khodabandeh A, Fesharaki MH, Champliaud H, Jahazi M. Local mechanical properties, microstructure, and microtexture in friction stir welded Ti-6Al-4V alloy. Mater Sci Eng A 2019;749:166–75. https://doi.org/10.1016/j.msea.2019.01.077.

[46] Gili AB, Hattingh DG, Bernard D. Relationship between tool tilt angle, shoulder plunge depth and process energy input for pin-less friction stir welded thin Ti-6Al-4V sheets. IOP Conf Ser Mater Sci Eng 2019;655:012010. https://doi.org/10.1088/1757-899X/655/1/012010.

[47] Buffa G, Fratini L, Micari F. Mechanical and microstructural properties prediction by artificial neural networks in FSW processes of dual phase titanium alloys. J Manuf Process 2012;14:289–96. https://doi.org/10.1016/j.jmapro.2011.10.007.

[48] Buffa G, Fratini L, Micari F, Settineri L. On the choice of tool material in friction stir welding of titanium alloys. Proc. NAMRI/SME, vol. 40, 2012, p. 785–94.

[49] Qi Y, Li J, Shen Y, Hou W. Simulation and Experimental Study on Temperature and Flow Field in Friction Stir Welding of TC4 Titanium Alloy Process. Mater Trans 2020;61:2378–85. https://doi.org/10.2320/matertrans.MT-M2020017.

[50] Yue Y, Wen Q, Ji S, Ma L, Lv Z. Effect of Temperature Field on Formation of Friction Stir Welding Joints of Ti–6Al–4V Titanium Alloy. High Temp Mater Process 2017;36:733–9. https://doi.org/10.1515/htmp-2015-0178.

[51] ASTM International. Standard Practice for Microetching Metals and Alloys ASTM E407 2016;07:1–22. https://doi.org/10.1520/E0407-07R15E01.2.

[52] ASTM International. Standard Test Methods for Vickers Hardness and Knoop Hardness of Metallic Materials ASTM E92 2017. https://doi.org/10.1520/E0092-17.

[53] ASM Specification Aerospace Metals. Titanium Grade 5. Last time accessed on August 31 2022 n.d. https://asm.matweb.com/search/SpecificMaterial.asp?bassnum=mtp641.

[54] ASM Specification Aerospace Metals. Titanium Grade 2. Last time accessed on August 31 2022 n.d. https://asm.matweb.com/search/SpecificMaterial.asp?bassnum=MTU020.

[55] Tarín P, Gualo A, Simón AG, Piris NM, Badía JM. Study of Alpha-Beta Transformation in Ti-6Al-4V-ELI. Mechanical and Microstructural Characteristics. Mater Sci Forum 2010;638–642:712–7. https://doi.org/10.4028/www.scientific.net/MSF.638-642.712.

[56] Murugesh L, Ravi J, Mahmood ST, Murty KL. Contractile strain ratios of textured cp-titanium (Grade II) sheet. J Mater Shap Technol 1989;7:81–90. https://doi.org/10.1007/BF02833774.

[57] Gupta RK, Kumar VA, Mathew C, Rao GS. Strain hardening of Titanium alloy Ti6Al4V sheets with prior heat treatment and cold working. Mater Sci Eng A 2016;662:537–50. https://doi.org/10.1016/j.msea.2016.03.094.

[58] Oliveira JP, Shen J, Escobar JD, Salvador CAF, Schell N, Zhou N, et al. Laser welding of H-phase strengthened Ni-rich NiTi-20Zr high temperature shape memory alloy. Mater Des 2021;202:109533. https://doi.org/10.1016/j.matdes.2021.109533.

[59] Oliveira JP, Shamsolhodaei A, Shen J, Lopes JG, Gonçalves RM, de Brito Ferraz M, et al. Improving the ductility in laser welded joints of CoCrFeMnNi high entropy alloy to 316 stainless steel. Mater Des 2022;219:110717. https://doi.org/10.1016/j.matdes.2022.110717.